

# Thermodynamic Modeling of Multi-component Calcium Ferrite for Sintering Reaction Analysis

Reiko MURAO\*  
Masao KIMURA

In-Ho JUNG

## Abstract

*The thermodynamic model of silico-ferrites of calcium and aluminum solution, the SFCA phase ( $\text{Ca}_2(\text{Fe}, \text{Ca})_6^{\text{Oct}}(\text{Fe}, \text{Al}, \text{Si})_6^{\text{Tet}}\text{O}_{20}$ ), was newly developed in the framework of the Compound Energy Formalism (CEF). Preferred substitution of Al atoms to tetrahedral sites in the SFCA solution was verified by X-ray absorption near edge structure (XANES) analysis. When considering crystallographic information in particular the short-range-ordering nature in the SFCA solution, the  $\text{Ca}_8(\text{Fe}^{3+})_{20}^{\text{Oct}}(\text{CaSi}^{6+}, \text{FeFe}^{6+}, \text{FeAl}^{6+})_3^{\text{Paired}}(\text{CaSi}^{6+})_1^{\text{Paired}}(\text{Fe}^{3+}, \text{Al}^{3+})_{20}^{\text{Tet}}\text{O}_{80}$  structure was considered for modeling the SFCA solution. The optimized Gibbs energies of all end-members can successfully reproduce the experimental single phase region of the SFCA solution.*

## 1. Introduction

In the industrial sintering process, fine ores are mixed with limestone flux and coke breeze, and heated by the combustion of coke breeze in a temperature range of 1450 to 1600 K for a few minutes. This generates Ca-Fe-O melt and allows for the melt of ore powder. In the cooling process, the solid phases precipitated from the Ca-Fe-O melt are calcium ferrites ( $\text{CaO-Fe}_2\text{O}_3$ ), multi-component calcium ferrites (silico-ferrites of calcium and aluminum), secondary hematite, magnetite, amorphous calcium silicate ( $\text{CaO-SiO}_2$ ) and the solid solution of them. These form a complex micro-texture mixed with iron ore grains, pores, and cracks. These phases play an important role in providing appropriate sinter properties such as strength or reducibility.<sup>1,2)</sup> The composition and quantity of liquid formed during the sintering process are affected by various process factors such as the heat pattern, composition of sinter, and oxygen partial pressure near the grain boundary of iron ore grains.

Although the sintering reaction is a non-equilibrium and inhomogeneous, it is important to understand solid-liquid equilibrium of the sinter ore system for the quantitative analysis and verification of these factors. The sintered reaction has diffusion limitation and it progresses with an uneven non-equilibrium reaction. By considering only a system with a very narrow range, the reaction can be realized through local thermodynamic equilibrium. For example, in the refining process, process simulation is performed using the Effective

Equilibrium Reaction Zone Model.<sup>3,4)</sup> Our research group is trying to establish a multi-component system phase diagram in parallel with the reaction dynamics analysis<sup>5,6)</sup> using the X-ray diffraction (XRD) and the X-ray absorption spectroscopy (XAS).

For the experimental phase diagram, the quasi-binary system such as the  $\text{Fe}_2\text{O}_3\text{-CaO}$  system has been studied thoroughly.<sup>7)</sup> However, the multi-component-based high  $\text{FeO}_x$  region including ore composition of  $\text{SiO}_2$ ,  $\text{MgO}$ , etc. remains unclear. For the  $\text{CaO-Fe}_2\text{O}_3\text{-SiO}_2$  quasi-ternary system, the region with oxygen partial pressure of  $10^{-3}$  Pa from the atmospheric pressure has been experimentally studied by Kimura, et al.<sup>8)</sup> The most recent report of the high  $\text{Fe}_2\text{O}_3$  region for  $\text{Al}_2\text{O}_3\text{-CaO-Fe}_2\text{O}_3$  at 1573 K was prepared in 1967, and the existence of various ternary system solid phases was shown.<sup>9)</sup> For the liquid phase region for the  $\text{Al}_2\text{O}_3\text{-CaO-Fe}_2\text{O}_3\text{-SiO}_2$  quasi-quaternary system, only the low  $\text{Al}_2\text{O}_3$  region with about 5 mass% has been studied. In the  $\text{Al}_2\text{O}_3\text{-CaO-Fe}_2\text{O}_3\text{-SiO}_2$  quasi-quaternary system, the continuous solid phase of compound multi-component calcium ferrite (SFCA: silico-ferrites of calcium and aluminum) is generated.

The single crystal structure analysis result of at least three types of multi-component calcium ferrite, the so-called SFCA ( $\text{A}_2\text{T}_6\text{M}_6\text{O}_{20}$ ), SFCA-I ( $\text{A}_3\text{BM}_8\text{T}_8\text{O}_{28}$ ), and SFCA-II ( $\text{A}_4\text{T}_{14}\text{M}_{16}\text{O}_{48}$ ) phase, which are a homologous series based on that of aenigmatite, has been reported.<sup>10-14)</sup> In the structure formula,  $\text{A}=\text{Ca}^{2+}$ ,  $\text{B}=\text{Ca}^{2+}$ ,  $\text{Fe}^{2+}$ , and  $\text{M}$

\* Senior Researcher, Dr. Eng., Materials Characterization Research Lab., Advanced Technology Research Laboratories  
20-1 Shintomi, Futtsu City, Chiba Pref. 293-8511

and T indicate the octahedral 6-coordination and the tetrahedral 4-coordination cation sites, respectively. The stable regions of these phases were experimentally researched by Patrick, et al., but have not yet been completely clarified, as shown in Fig. 1<sup>15)</sup>. The homogeneity range of the SFCA-I and SFCA-II phases is still under discussion.<sup>16)</sup> The Si-free SFCA-II is a ternary solid solution with a compositional range of Fe<sub>2</sub>O<sub>3</sub> between 44.5 and 81.5 mol%, according to Dayal, et al.<sup>9,16)</sup> Patrick, et al. also reported the possibility of substitution of the SFCA-I and SFCA-II phases.<sup>17)</sup>

The crystal structures of the SFCA, SFCA-I, and SFCA-II phases can be described as the sequences of pyroxene (P) and spinel (S) modules. The SFCA phase has the P-S-P-S- cycle, and its composition is a high-Si and low-Fe type with a wide range of Al<sub>2</sub>O<sub>3</sub> substitution. The SFCA-I phase has the P-S-S-P-S-S- cycle and its composition is a low-Si and high-Fe type compared to the SFCA phase.<sup>12)</sup> The structure of the Si-free SFCA-II is determined by the single crystal X-ray diffraction analysis, and its structure indicates the features of both the SFCA and SFCA-I type, resulting in the P-S-P-S-S- cycle.<sup>13)</sup>

In the case of a multi-component system, it is difficult to clarify all the complex phase equilibria between solid and liquid phases under different partial pressure of oxygen. Therefore, the CALPHAD-type thermodynamic database, which is constructed based on the critical evaluation and optimization of all the reliable thermodynamic and phase diagram data in the literature, can be a very useful tool for identifying complex phase equilibrium in the composition and partial pressure condition of interest. The FactSage thermodynamic database<sup>18,19)</sup> has been built for the past several decades and widely applied to the pyrometallurgical processes including ironmaking and steelmaking.<sup>20)</sup> Regarding the Al<sub>2</sub>O<sub>3</sub>-CaO-Fe<sub>2</sub>O<sub>3</sub>-SiO<sub>2</sub> system, in particular for iron sinter ore application, however, the SFCA phase that is one of the key sinter phases is missing in the database.

This study proposes a thermodynamic model of the SFCA solution phase in the Al<sub>2</sub>O<sub>3</sub>-CaO-Fe<sub>2</sub>O<sub>3</sub>-SiO<sub>2</sub> system. For a thorough explanation of the thermodynamic nature of the SFCA phase, the crystal structure of the SFCA phase should be taken into account in the CALPHAD-type modeling. Although the crystal structure of the SFCA has already been determined via single X-ray diffraction analysis,<sup>11)</sup> the distribution of Al has been unclear especially for the high-Al-bearing SFCA phase. Therefore, in the present study, the X-ray absorption near edge structure (XANES) of the SFCA phase prepared with the powder sintering method was also investigated to

analyze the coordination environment of cations. The thermodynamic model parameters of the SFCA phase were optimized to reproduce the liquid- and solid-phase equilibria related to the SFCA phase in the Al<sub>2</sub>O<sub>3</sub>-CaO-Fe<sub>2</sub>O<sub>3</sub>-SiO<sub>2</sub> system in air. The FactSage ver. 6.4 FToxid database was used for all solid and liquid phases other than the SFCA phase.

## 2. Experimental and Thermodynamic Calculations

### 2.1 Sample preparation

Three SFCA samples with different compositions were prepared by the conventional powder sintering method for X-ray absorption measurements. Starting materials α-Fe<sub>2</sub>O<sub>3</sub> (4N grade, 1 μm), CaCO<sub>3</sub> (4N grade, 12 μm), α-SiO<sub>2</sub> (99%, 1 μm), and α-Al<sub>2</sub>O<sub>3</sub> (4N grade, 1 μm) were mixed with an agate pestle and mortar with the nominal compositions shown in Table 1<sup>15)</sup>. Each sample of 1 g was pressed into pellets having a diameter of 13 mm at a pressure of 24 MPa. These pellets were calcined at 1070 K for 10 h for decarbonation, then crushed, pelletized, and sintered at 1500 K over 60 h in a platinum crucible to confirm products as single phases by powder X-ray diffraction measurements and check those compositions via X-ray fluorescent analysis. The reference material FePO<sub>4</sub> was prepared by dehydration of FePO<sub>4</sub>·nH<sub>2</sub>O at 870 K. Ca<sub>2</sub>Fe<sub>2</sub>O<sub>5</sub>, CaFe<sub>2</sub>O<sub>4</sub>, and Ca<sub>2</sub>(Fe, Al)<sub>2</sub>O<sub>5</sub> were prepared by the same process of SFCA with the sintering temperature of 1370 K.

### 2.2 X-ray absorption measurements

XAFS experiments were conducted at Photon Factory, KEK (KEK-PF), Japan. Al K-edge XANES spectra were collected at BL-11A by the total electric yield (TEY) method. The energy scale was calibrated at 1s → t<sub>1u</sub> peak top of the Al K-edge absorption of α-Al<sub>2</sub>O<sub>3</sub> as 1568.7 eV.

Fe K-edge XANES spectra were collected at BL-9A by a transmitting method. Synthesized SFCA and reference materials were ground into powder of 10 mm diameter pellets and diluted with BN powder for the X-ray absorption measurements so that the absorption difference Δμt before and after absorption edge may be about 1. The energy scale was calibrated at the minimum point of the first differential curve of edge absorption of Fe foil as 7113.2 eV. Normalized XANES spectra data (Δμt=1) were used to calculate the integrated intensity of the pre-edge peak of Fe K-edge.

### 2.3 FactSage thermodynamic databases

Phase equilibrium calculations of the Al<sub>2</sub>O<sub>3</sub>-CaO-Fe<sub>2</sub>O<sub>3</sub>-SiO<sub>2</sub> system were conducted by using the thermodynamic database with Gibbs energy minimization software, FactSage 6.4. The FactSage FToxid database was used for various solid and liquid oxide phases other than the SFCA phase, and FactPS (pure substances database) was used for gas phases to fix the oxygen partial pressure.

The Modified Quasi-chemical Model (MQM) is used in the FToxid database for the multi-component molten oxide solution.<sup>21,22)</sup> The MQM can reproduce the oxygen bonding structure in molten oxide. For example, the network breaking reaction of SiO<sub>2</sub> by a network modifier (MO) can be well reproduced in the MQM by the (Si-O-Si) + (M-O-M) = 2 (Si-O-M) pair exchange reaction between

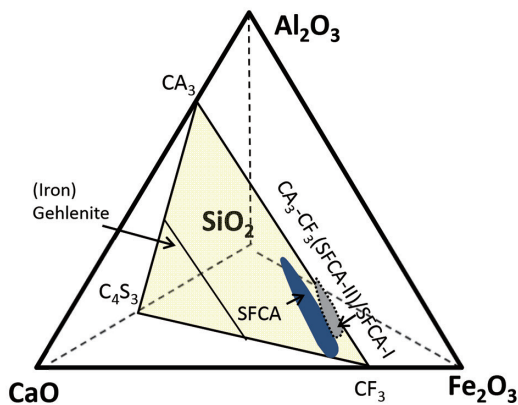


Fig. 1 Schematic phase diagram indicating the CaAl<sub>6</sub>O<sub>10</sub>-Ca<sub>4</sub>Si<sub>3</sub>O<sub>10</sub>-CaFe<sub>6</sub>O<sub>10</sub> (CA3-C4S3-CF3) plane, the SFCA single phase region in the Al<sub>2</sub>O<sub>3</sub>-CaO-Fe<sub>2</sub>O<sub>3</sub>-SiO<sub>2</sub> system<sup>15)</sup>

Table 1 Chemical compositions of sintered SFCA (mol%)<sup>15)</sup>

Sample	Fe <sub>2</sub> O <sub>3</sub>	CaO	Al <sub>2</sub> O <sub>3</sub>	SiO <sub>2</sub>
SFCA05	56.1	30.4	5.7	7.9
SFCA15	50.4	27.3	17.1	5.2
SFCA30	37.2	25.8	32.2	4.9

the second nearest cations, which is a key to reproducing the entropy of mixing. Many binary and ternary liquid solutions have been modeled using the MQM and the Gibbs energies of the liquid solutions in higher-order systems are properly predicted from the model parameters of the binary and ternary systems.

The Compound Energy Formalism (CEF)<sup>23,24</sup> has been used to describe complex solid solutions. In the CEF, the crystallographic information, in particular the mixing of cations (species), at a given sublattice is properly taken into account for better reproduction of entropy of solid solution. In this study, the SFCA phase was newly modeled in the framework of the CEF taking into account its crystallographic features. All thermodynamic calculations in this study were performed using the FactSage software 6.4 version.

### 3. Results

#### 3.1 XANES analysis

**Figure 2**<sup>15</sup> shows the normalized Al *K*-edge XANES spectra of the SFCA and reference materials ( $\text{AlPO}_4$ ,  $\alpha\text{-Al}_2\text{O}_3$ ,  $\text{MgAl}_2\text{O}_4$ ,  $\text{Al}_4\text{Si}_4\text{O}_{10}(\text{OH})_8$ , and  $\text{Ca}_2(\text{Fe},\text{Al})_2\text{O}_5$ ). Three SFCA phases and  $\text{Ca}_2(\text{Fe},\text{Al})_2\text{O}_5$  indicate pre-edge peak characteristics of Al in oxygen tetrahedral coordination at 1563.5 eV. If the Al structure is oxygen hexahedral, the absorption peak is predicted to be around 1569 eV. It was difficult to directly determine whether Al is distributed in the oxygen hexahedral sites from these spectra due to the broad shoulder observed around 1575 to 1567 eV in the SFCA phase spectra. To analyze the structure in detail, multiple scattering analysis using the crystal structure model is required.

**Figure 3**<sup>15</sup> shows the normalized Fe *K*-edge XANES spectra of the SFCA and reference materials. Pre-edge peaks due to  $1s$  to  $3d$  forbidden transition were observed around an energy of 7108 eV and those energy positions were almost the same as those in the

SFCA phase with a reference containing  $\text{Fe}^{3+}$ . The energy position of the pre-edge peak of Fe *K*-edge absorption depends on the valence of the Fe ion and its peak intensity is stronger in tetrahedral 4-coordination with lower symmetry than in octahedral 6-coordination with higher symmetry.<sup>25</sup>

In the case of powder sintering in an air atmosphere, the SFCA with a low  $\text{Fe}^{2+}/\text{Fe}^{3+}$  ratio of about 0.02 was formed<sup>14</sup> and the presence of  $\text{Fe}^{2+}$  was ignored in this analysis. The peak profile of pre-edge was fitted by the Gaussian function after spline fitting of the baseline and an integrated peak intensity was obtained. **Figure 4**<sup>15</sup> (a) shows the pre-edge peak height of normalized spectra for each specimen. The pre-edge intensity of  $\text{FePO}_4$ , which has one oxygen tetrahedral coordinated site of Fe, was the highest among specimens. The lowest peak intensity was obtained for  $\text{CaFe}_2\text{O}_4$  and  $\alpha\text{-Fe}_2\text{O}_3$ , which have only hexahedral-coordinated sites of Fe.  $\text{Ca}_2\text{Fe}_2\text{O}_5$  has one hexahedral- and one tetrahedral-coordinated site, so that the pre-edge intensity was in the middle among the reference materials. The SFCA structure has six tetrahedral-coordinated cation sites and six hexahedral-coordinated cation sites.

Fe atoms are distributed in both sites, while Si atoms occupy only tetrahedral sites. Ca atoms are distributed in two 7-coordinated sites and hexahedral sites. On the contrary, Al is amphoteric and may be distributed in both tetrahedral and hexahedral sites. This may depend on the coordination environment of each site such as cation-oxygen distances. To determine the distribution of Al in hexahedral and tetrahedral sites in the SFCA structure, a quadratic correlation equation between the ratio of Fe occupying the hexahedral sites and tetrahedral sites to the total Fe and integrated pre-edge peak intensity was obtained from the data set of  $\text{FePO}_4$ ,  $\text{Ca}_2\text{Fe}_2\text{O}_5$ ,  $\text{CaFe}_2\text{O}_4$ , and  $\alpha\text{-Fe}_2\text{O}_3$ , as shown in Fig. 4(b). The distribution of Fe,

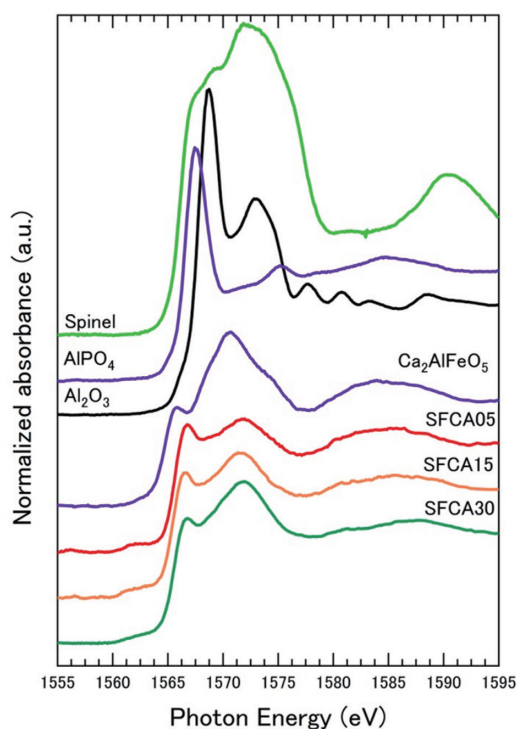


**Fig. 2** Al *K*-edge XANES spectra of spinel,  $\text{AlPO}_4$ ,  $\text{Al}_2\text{O}_3$ ,  $\text{Ca}(\text{Fe}_{0.5}\text{Al}_{0.5})_2\text{O}_5$ , SFCA05, SFCA15 and SFCA30<sup>15</sup>

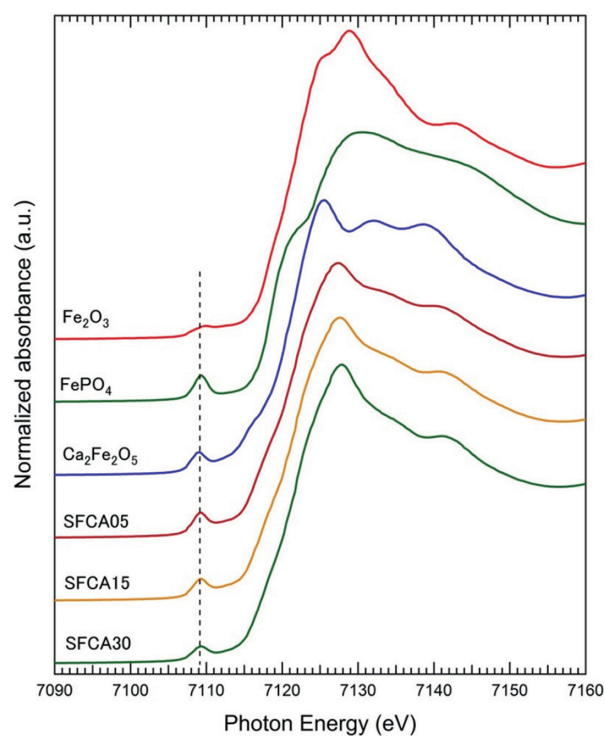


**Fig. 3** Fe *K*-edge XANES spectra of  $\text{Fe}_2\text{O}_3$ ,  $\text{FePO}_4$ ,  $\text{Ca}_2(\text{Fe}_{0.5}\text{Al}_{0.5})_2\text{O}_5$ , SFCA05, SFCA15 and SFCA30<sup>15</sup>. Dashed line indicates the pre-edge peak position.

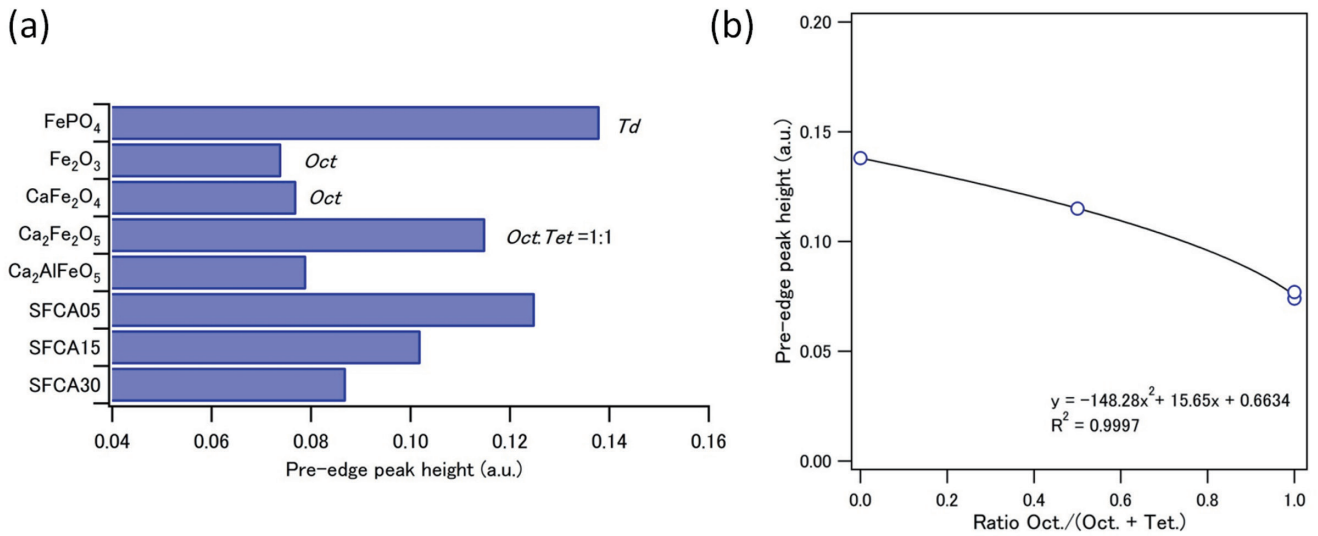


Fig. 4 (a) Pre-edge peak height of FePO<sub>4</sub>, Fe<sub>2</sub>O<sub>3</sub>, CaFe<sub>2</sub>O<sub>4</sub>, Ca<sub>2</sub>Fe<sub>2</sub>O<sub>5</sub>, Ca<sub>2</sub>(Fe<sub>0.5</sub>Al<sub>0.5</sub>)<sub>2</sub>O<sub>5</sub>, SFCA05, SFCA15 and SFCA30 (b) Relation between the atomic ratio of iron in octahedral site to total (octahedral+tetrahedral) iron and the pre-edge peak height of normalized Fe K-edge XANES spectra<sup>15)</sup>

Table 2 Distribution of cations in octahedral and tetrahedral sites and distribution of Fe determined via Fe K-edge XANES analysis<sup>15)</sup>

Sample	Site occupancy of cation (a.p.f.u.)						Ratio of Fe <sup>3+</sup>		
	Octahedral sites			Tetrahedral sites			Total Fe <sup>3+</sup>	Oct./(Oct+Tet)	
	Ca <sup>2+</sup>	Fe <sup>3+</sup>	Al <sup>3+</sup> (fixed)	Fe <sup>3+</sup>	Si <sup>4+</sup>	Al <sup>3+</sup>		Calcd.	XANES
SFCA05	0.67	5.33	0	4.34	0.67	0.99	9.66	0.55	0.3
SFCA15	0.43	5.57	0	2.75	0.43	2.83	8.32	0.67	0.72
SFCA30	0.39	5.61	0	0.4	0.39	5.21	6	0.93	0.9
Ca <sub>2</sub> (Fe,Al) <sub>2</sub> O <sub>5</sub>	–	1	0	0	–	1	1	1	0.97

and subsequently Al, in hexahedral and tetrahedral sites can be determined.

Table 2<sup>15)</sup> shows the types and the calculated distribution of cations (a.p.f.u.) in the hexahedral and tetrahedral sites and the ratio of hexahedral site occupancy of all Fe, assuming all Al atoms are in tetrahedral sites. The right column shows the ratio of hexahedral site occupancy of Fe determined via XANES pre-edge peak intensity analysis. The XANES analysis results agreed well with the assumption of preferred substitution of Al in tetrahedral sites. In the case of SFCA30, which is at the almost maximum limit of the Al solid solution-range, most of Fe is distributed in hexahedral sites, which means that the stable compositional range of the SFCA phase is limited by the substitution limit of Al in the tetrahedral site.

As a result of the XANES analysis, the SFCA solid solution can be expressed as Ca<sub>2</sub>(Fe, Ca)<sub>6</sub><sup>Oct</sup>(Fe, Al, Si)<sub>6</sub><sup>Tet</sup>O<sub>20</sub>.

### 3.2 Thermodynamic modeling of SFCA

The thermodynamic model of the SFCA solution was developed in the framework of the CEF. Several sublattice structures were tested for describing the SFCA solution. As the thermodynamic properties of the SFCA solution have not been determined, the model was verified to reproduce the phase equilibria between liquid and SFCA by Patrick, et al.<sup>17)</sup>

The Gibbs energy of an oxide solid solution can be described by the CEF considering its crystallographic nature. Let's assume the crystal structure of the solution is A<sub>a</sub>(X, Y)<sub>m</sub><sup>O</sup>(M, N)<sub>n</sub><sup>T</sup>O<sub>2</sub>, where a, m, n,

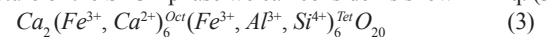
and z represent the number of sublattices per formula unit. X and Y cations can occupy "O" sublattices and M and N cations "T" sublattices. Then, Gibbs energy G<sup>m</sup> of this solid solution per formula can be expressed as follows using the CEF:

$$G^m = \sum_i \sum_j Y_i^O Y_j^T G_{ij} - TS_c + G^E \quad (1)$$

$$S_c = -R (m \sum_i Y_i^O \ln Y_i^O + n \sum_j Y_j^T \ln Y_j^T) \quad (2)$$

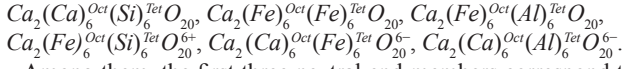
where Y<sub>i</sub><sup>O</sup> and Y<sub>j</sub><sup>T</sup> are the site fraction of i and j cations in the "O" and "T" sites. G<sub>ij</sub> represents the molar Gibbs energy of A<sub>a</sub>(i)<sub>m</sub><sup>O</sup>(j)<sub>n</sub><sup>T</sup>O<sub>z</sub> end-member of the solution. S<sub>c</sub> is the configuration entropy of solution which is calculated based on the random mixing of species at O and T sites, where m and n are the number of moles of the O and T sublattices, respectively. That is, for the CEF, the random mixing of species at a given sublattice is considered. G<sup>E</sup> is the excess Gibbs energy, which includes the interaction energy between the mixing species in the solution. The main model parameters in the CEF are the Gibbs energy of end-member, G<sub>ij</sub>. In particular, as some of the end-members in the Gibbs energy description can be imaginary pseudo-components, their Gibbs energy values can directly influence the Gibbs energy of the solution.

If necessary, G<sup>E</sup> can be introduced to further refine the Gibbs energy of the solution. The simplest and most straightforward sublattice structure of the SFCA phase we can consider is shown in Eq. (3):



where only hexahedral and tetrahedral sites are substituted with the

different cations. Then, the molar Gibbs energy,  $G^m$ , of the SFCA solution per formula can be described using Eqs. (1) and (2). Under this formula, six end-members can be defined:



Among them, the first three neutral end-members correspond to the composition of  $Ca_4Si_3O_{10}$ ,  $CaFe_6O_{10}$ , and  $CaFe_3Al_3O_{10}$ , in the phase diagram of the  $CaAl_6O_{10}$ - $Ca_4Si_3O_{10}$ - $CaFe_6O_{10}$  system, as shown in Fig. 1. The other 3-charged end-members do not appear in the diagram. Using the formula in Eq. (3), it was very difficult to obtain the homogeneity range of the SFCA solid solution of up to 35 mol% of  $CaAl_6O_{10}$  in the  $CaAl_6O_{10}$ - $Ca_4Si_3O_{10}$ - $CaFe_6O_{10}$  system.

The only way to increase the homogeneity range toward  $CaAl_6O_{10}$  of the SFCA phase was to stabilize the pseudo-end-member  $Ca_2(Fe)_6^{Oct}(Al)_6^{Tet}O_{20}$  by decreasing its Gibbs energy. However, this would cause the formation of stable  $CaFe_3Al_3O_{10}$  in the  $CaFe_6O_{10}$ - $CaAl_6O_{10}$  section. In addition, it was difficult to control the solubility of Si in the SFCA structure within the experimentally measured concentration range (Si=0.25 to 1.0 mole per mole of  $(Ca_2(X)_6^{Oct}(Y)_6^{Tet}O_{20})$ )<sup>13</sup> which was obtained mainly by adjusting the Gibbs energy of  $Ca_2(Ca)_6^{Oct}(Si)_6^{Tet}O_{20}$ .

There is a charge compensation relationship,  $(Ca^{2+})^{Oct} + (Si^{4+})^{Tet} = (Fe^{3+})^{Oct} + (Fe^{3+}, Al^{3+})^{Tet}$  in the SFCA structure. That is, when  $Si^{4+}$  dissolves in tetrahedral sites with the replacement of  $Fe^{3+}$  or  $Al^{3+}$ ,  $Ca^{2+}$  should be dissolved in the hexahedral site by replacing  $Fe^{3+}$  for balancing.

Figure 5<sup>15</sup> shows the crystal structure of the SFCA phase based on the crystallographic data reported by Hamilton, et al.<sup>11</sup>  $Si^{4+}$  was concentrated at a certain tetrahedral site and was located close to the hexahedral site with  $Ca^{2+}$  concentrated. This means that the sublattice structure used in the above SFCA model (3) is improper and the entropy of mixing of real solution is overestimated. To describe such a short-range-ordering behavior between  $Si^{4+}$  and  $Ca^{2+}$  in the SFCA structure, a pair of the tetrahedral and the hexahedral sites can be considered as one of the sublattices. The SFCA phase solid solution range of  $Si^{4+}$  in an air atmosphere ranges between 0.25 and 1.0 atom per six tetrahedral-coordinate sites<sup>14</sup>. That is, the maximum  $Si^{4+}$  occupancy in tetrahedral sites is 1/6, and 1, out of 6, tetrahedral and hexahedral sites were considered as the paired sites.

In the paired sites, CaSi, FeFe, and FeAl pairs can exist assuming the cation species in the hexahedral and the tetrahedral sites (Ca and Fe in hexahedral sites and Fe, Al, and Si in tetrahedral sites). In particular, no CaFe, CaAl, and FeSi pairs were considered in the paired sites to ensure that all Ca are paired with Si. There are one-

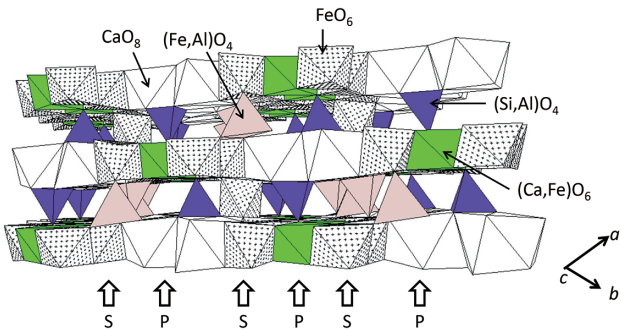
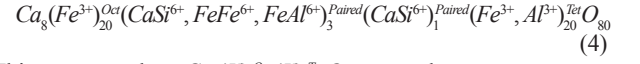


Fig. 5 Schematic of the crystal structure of SFCA<sup>11</sup> indicating spinel (S) and pyroxene (P) modules, and the short-range-ordering of Si and Ca in tetrahedral (Si,Al)O<sub>4</sub> sites and octahedral (Ca,Fe)O<sub>6</sub> sites, respectively<sup>15</sup>

mole paired sites per mole of SFCA solution with  $Ca_2(X)_6^{Oct}(Y)_6^{Tet}O_{20}$ . Among the one-mole paired sites, a quarter of them were again occupied only for CaSi such that the solubility of Si in SFCA can vary from 0.25 mole per mole of  $Ca_2(X)_6^{Oct}(Y)_6^{Tet}O_{20}$ . The rest of the hexahedral sites were assumed to be occupied only by Fe, and the rest of the tetrahedral sites were occupied by Fe and Al.

In summary, the modified crystal structure of the SFCA phase is shown in Eq. (4) as follows:



This corresponds to  $Ca_8(X)_{24}^{Oct}(Y)_{24}^{Tet}O_{80}$  per mole.

There are six end-members to express the modified SFCA solution with the above-mentioned crystal structure using the CEF. Figure 6<sup>15</sup> (a) shows a schematic illustration of the end-members in the bi-pyramid structure, and Fig. 6 (b) shows the compositions of the end-members plotted on the  $CaAl_6O_{10}$ - $Ca_4Si_3O_{10}$ - $CaFe_6O_{10}$  (CA3-C4S3-CF3) plane. In Fig. 6(b), the circles and triangles indicate a single-phase SFCA region that was experimentally confirmed.<sup>17,26</sup> It should be noted that the compositional range of the end-members in the SFCA solution is wide enough to contain all the experimental single-phase SFCA compositions, and all the end-members are charged to neutral.

In the formula of the SFCA solution in Eq. (4), let us define 3 moles of paired sites containing CaSi, FeFe, and FeAl as P sites, and 20 moles of tetrahedral sites containing Fe and Al as the T site for the sake of simplicity. According to Eqs. (1) and (2), the molar Gibbs energy of the SFCA solution per mole of  $Ca_8(X)_{24}^{Oct}(Y)_{24}^{Tet}O_{80}$  can be expressed as follows:

$$G^m = \sum_i Y_i^P Y_j^T G_{ij} - TS_c + G^E \quad (5)$$

$$S_c = -R(3 \sum_i Y_i^P \ln Y_i^P + 20 \sum_j Y_j^T \ln Y_j^T) \quad (6)$$

where  $Y_i^P$  and  $Y_j^T$  are the occupancy of the  $i$ -th and the  $j$ -th cations in the P and T sites, respectively, and  $G_{ij}$  is the molar Gibbs energy of the end-member  $Ca_8(Fe^{3+})_{20}^{Oct}(i)_3^{Paired}(CaSi^{6+})_1^{Paired}(j)_{20}^{Tet}O_{80}$ . The configuration entropy,  $S_c$ , is also defined as shown in Eq. (6).

In expressing the solution using the CEF, the molar Gibbs energy of six end-members  $G_{ij}$  is the most important model parameter. None of  $G_{ij}$  in the present formula is the actual stable phase in the  $CaAl_6O_{10}$ - $Ca_4Si_3O_{10}$ - $CaFe_6O_{10}$  system. Therefore, logical determination of  $G_{ij}$  is essential to accurately express the Gibbs energy of the SFCA solution. In the present study,  $G_{ij}$  (in the following expression, it is presented as  $G^o(i^P j^T)$ ) was defined using the well-known molar Gibbs energies of stable compounds such as  $CaFe_4O_7$ ,  $CaAl_4O_7$ ,  $Ca_3Si_2O_7$ ,  $CaSiO_3$ ,  $Fe_2O_3$ , or  $Al_2O_3$ :

$$G^o(CaSi^P Fe^T) = \frac{40}{6} G_{CF2}^o + \frac{8}{6} G_{C3S2}^o + \frac{8}{6} G_{CS}^o + \frac{40}{6} G_F^o + G_1 \quad (7)$$

$$\begin{aligned} &G^o(CaSi^P Al^T) \\ &= \frac{20}{6} G_{CF2}^o + \frac{20}{6} G_{CA2}^o + \frac{8}{6} G_{C3S2}^o + \frac{8}{6} G_{CS}^o + \frac{20}{6} G_F^o + \frac{20}{6} G_A^o + G_2 \quad (8) \end{aligned}$$

$$G^o(FeFe^P Fe^T) = \frac{46}{6} G_{CF2}^o + \frac{2}{6} G_{C3S2}^o + \frac{2}{6} G_{CS}^o + \frac{46}{6} G_F^o + G_3 \quad (9)$$

$$\begin{aligned} &G^o(FeFe^P Al^T) \\ &= \frac{26}{6} G_{CF2}^o + \frac{20}{6} G_{CA2}^o + \frac{2}{6} G_{C3S2}^o + \frac{2}{6} G_{CS}^o + \frac{26}{6} G_F^o + \frac{20}{6} G_A^o + G_4 \quad (10) \end{aligned}$$

$$\begin{aligned} &G^o(FeAl^P Fe^T) \\ &= \frac{43}{6} G_{CF2}^o + \frac{2}{6} G_{CA2}^o + \frac{2}{6} G_{C3S2}^o + \frac{2}{6} G_{CS}^o + \frac{43}{6} G_F^o + \frac{3}{6} G_A^o + G_5 \quad (11) \end{aligned}$$

$$\begin{aligned} &G^o(FeAl^P Al^T) \\ &= \frac{23}{6} G_{CF2}^o + \frac{23}{6} G_{CA2}^o + \frac{2}{6} G_{C3S2}^o + \frac{2}{6} G_{CS}^o + \frac{23}{6} G_F^o + \frac{23}{6} G_A^o + G_6 \quad (12) \end{aligned}$$

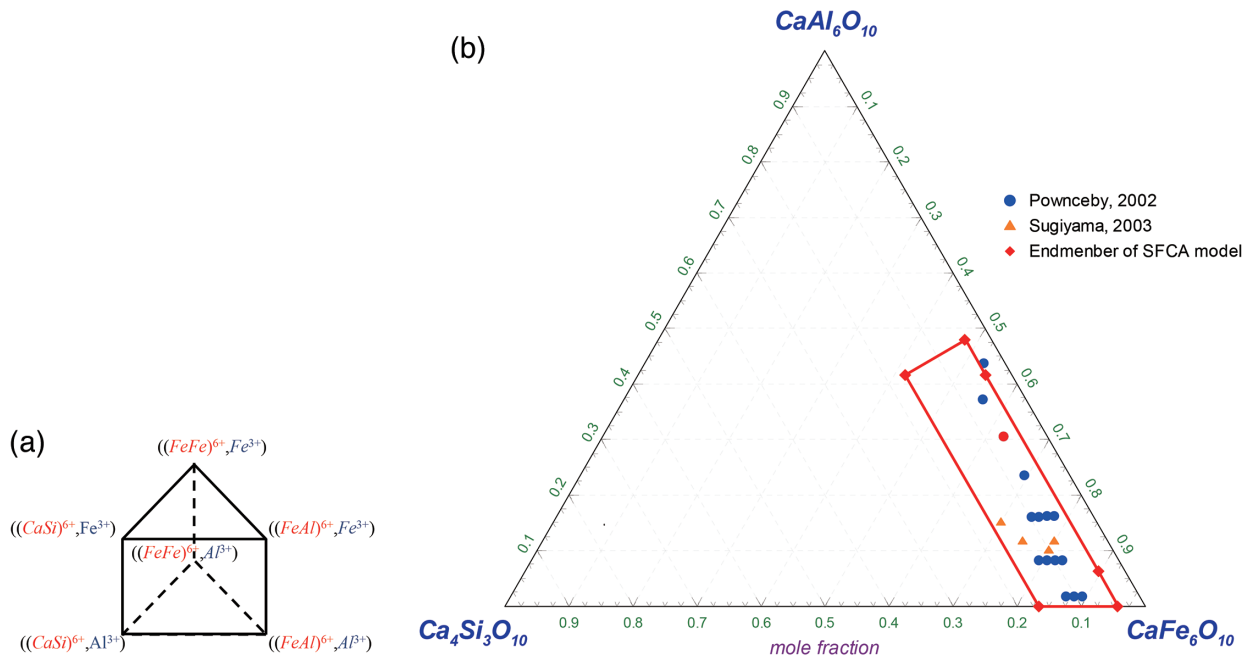


**Fig. 6** (a) Schematic of the Gibbs energy of end-members of SFCA solution model, and (b) Compositions of six end-members of the SFCA solution model on the  $\text{CaAl}_6\text{O}_{10}$ - $\text{Ca}_4\text{Si}_3\text{O}_{10}$ - $\text{CaFe}_6\text{O}_{10}$  (CA3-C4S3-CF3) plane<sup>15)</sup>  
 Circle and triangle symbols indicate the composition of single phase SFCA that were experimentally determined.<sup>17, 26)</sup>

where  $G_{CF2}^o$ ,  $G_{CA2}^o$ ,  $G_{C3S2}^o$ ,  $G_{CS}^o$ ,  $G_F^o$ , and  $G_A^o$  are the molar Gibbs energies of the  $\text{CaFe}_4\text{O}_7$ ,  $\text{CaAl}_4\text{O}_7$ ,  $\text{Ca}_3\text{Si}_2\text{O}_7$ ,  $\text{CaSiO}_3$ ,  $\text{Fe}_2\text{O}_3$ , and  $\text{Al}_2\text{O}_3$  phase, respectively. The expression of  $G^o(i^p j^q)$  with stable compounds was selected based on the numbers of respective cations and anions in the individual end-member.  $G_1$  to  $G_6$  are the additional Gibbs energy terms to adjust the value of  $G^o(i^p j^q)$ .

In this study,  $G^E$  was set to be zero in Eq. (5). Thus, the Gibbs energy of the SFCA solution can be fully expressed by the Gibbs energies of six end-members to reproduce the equilibrium between the single SFCA phase region and other phase regions.

### 3.3 Optimization of SFCA thermodynamic model

In this study, the surplus Gibbs energy terms of  $G_1$  to  $G_6$  in Eqs. (7) to (12) were optimized for the Gibbs energies of end-members of the SFCA solution model to reproduce experimental data, reported by Patrick, et al.<sup>17)</sup>, set in a temperature range between 1513 and 1663 K. The isothermal phase diagrams of the CA3-C4S3-CF3 system in an air atmosphere are acquired at 1513, 1543, 1573, and 1663 K as shown in Figs. 7<sup>15)</sup> (a) to (d) using the FToxid database and a new SFCA solution model with the optimized parameters. The colored regions in the figures show the calculated SFCA single-phase region.

The filled circles indicate the experimental data points of single-phase SFCA and the open circles indicate the mixtures of the SFCA and other phases, obtained based on the experiment by Patrick, et al.<sup>17)</sup> The filled triangles represent the mixtures of the SFCA and the meta-stable phase, possibly, due to the low temperature condition and short baking period of sample preparations. Experimental homogeneity areas of the SFCA phase (single phase region of SFCA) can be correctly calculated at temperatures between 1543 and 1663 K by the new SFCA model. Under the 1513 K condition, the single phase region of SFCA calculated in a low Al region ( $> 0.85\text{CF3}$ ) is slightly inconsistent with the experimental data; the calculated single phase region of SFCA in the low-CA3 region is extended more

toward the CF3 corner than the experimental one.

One possible reason for such inconsistency could be that in the thermodynamic model of the hematite ( $\alpha\text{-Fe}_2\text{O}_3$ ) phase used in these calculations, the solid solution of CaO in  $\text{Fe}_2\text{O}_3$  was not taken into consideration. In reality, approximately 10% of Fe is substituted with Ca in the hematite phase at 1513 K to form solid solution.<sup>27)</sup> This may destabilize the hematite phase and affect the single phase region of the SFCA phase. In addition, absence of the SFCA-I phase thermal model may also affect the stable region of the SFCA phase at around 0.85CF3.

The main focus of the present study is to develop the SFCA solution model using the CEF and optimize the model parameters. Although the generated region of the SFC phase was successfully reproduced by using the present SFCA model, the other phases around the SFCA require further examination. To this end, deeper research of the experimental phase diagram of the CA3-C4S3-CF3 system is also necessary. Another multi-component calcium ferrite with the aenigmatite-type structure, the SFCA-I phase, and the thermodynamic SFCA-II (i.e., C3) phase model with no  $\text{SiO}_2$  should be optimized to explain the phase equilibria involving the SFCA phase in the low  $\text{SiO}_2$  region. Further investigation of these matters is required in the near future.

## 4. Conclusions

A new thermodynamic model of the SFCA phase was developed in this study. It was confirmed via XANES analysis that Al atoms in the SFCA solution preferentially substitute tetrahedral sites. The thermodynamic model of Eq. (4) was developed in consideration of the short-range-ordering nature in the SFCA solution to model the SFCA solution crystallography based on the CEF. The optimized Gibbs energies of all end-members can successfully reproduce the single-phase region of the SFCA solution.

To analyze the real sintering process, the presence of  $\text{Fe}^{2+}$  or

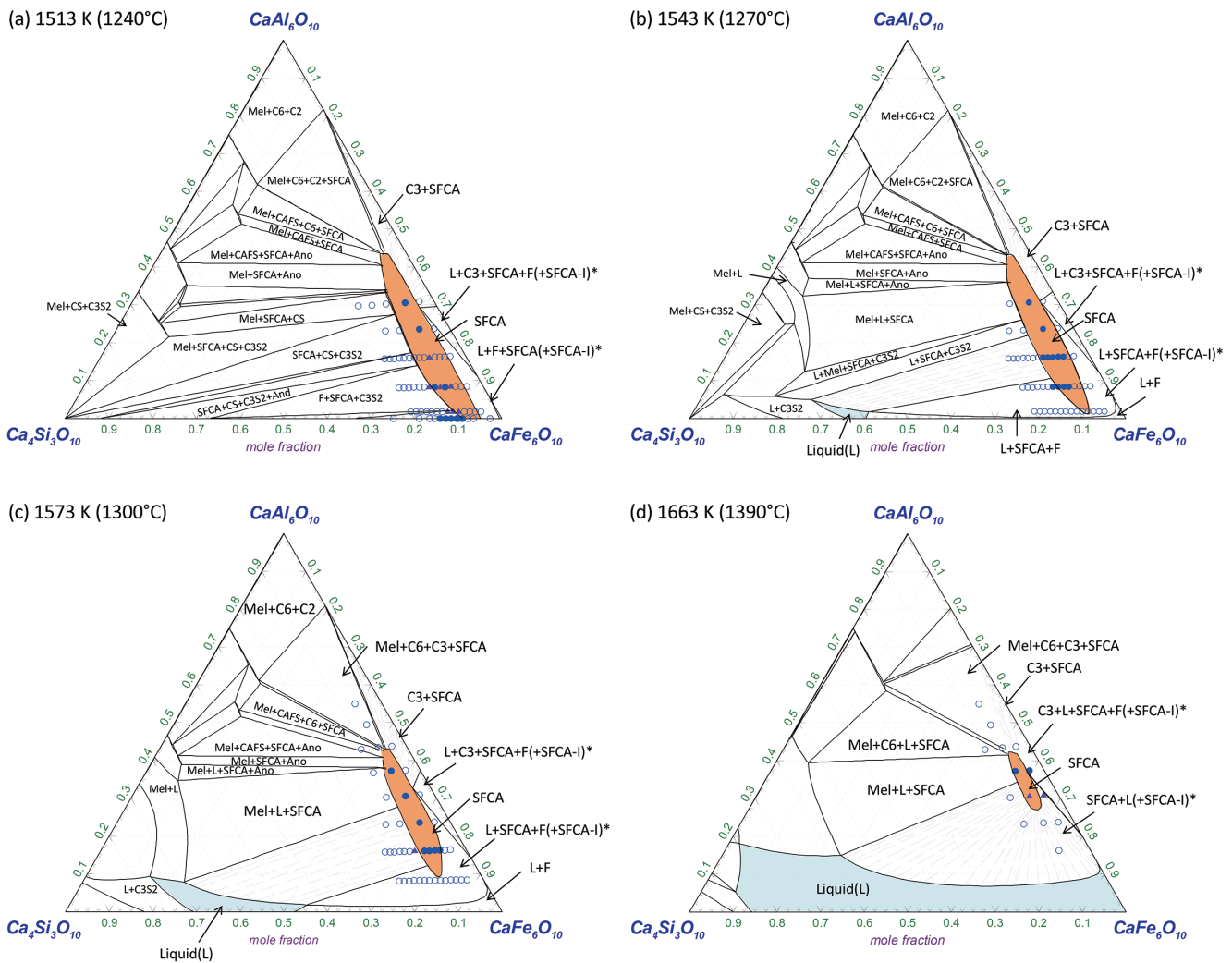


Fig. 7 Calculated isothermal phase diagrams of the CA3-C4S3-CF3 system using the present SFCA thermodynamic model at (a) 1513 K, (b) 1543 K, (c) 1573 K and (d) 1663 K, respectively<sup>15)</sup>

Painted regions show the calculated SFCA single-phase and liquidus region. Filled circles indicate experimental data points of single-phase SFCA, filled triangles represent the mixtures of the SFCA and the meta-stable phase and open circles indicate a mixture of SFCA and other phases reported by Patrick et al.<sup>17)</sup> F, CS, C3S2, And, and Ano stand for the stoichiometric  $\text{Fe}_2\text{O}_3$ ,  $\text{CaSiO}_3$ ,  $\text{Ca}_2\text{Si}_2\text{O}_7$ ,  $\text{Ca}_3\text{Fe}_2\text{Si}_3\text{O}_{12}$ , and  $\text{CaAl}_2\text{Si}_2\text{O}_8$ , respectively. Mel, CAFS, C6, C3, and C2 represent melilite,  $\text{Ca}_2(\text{Al,Fe})_8\text{SiO}_{16}$ ,  $\text{Ca}(\text{Al,Fe})_{12}\text{O}_{19}$ ,  $\text{Ca}(\text{Al,Fe})_6\text{O}_{10}$ , and  $\text{Ca}(\text{Al,Fe})_4\text{O}_7$  solid solution, respectively.

$\text{Mg}^{2+}$  should be taken into consideration. It was reported that the solution range of  $\text{Si}^{4+}$  and  $\text{Ca}^{2+}$  increases with the increase of  $\text{Mg}^{2+}$  concentration.<sup>14)</sup> The quantity of  $\text{Fe}^{2+}$  in the solution may increase in the SFCA phase, in particular, under low oxygen pressure. Further study on modeling of the remaining SFCA series including the SFCA-I phase is required. The re-optimization of the  $\text{CaO-SiO}_2\text{-FeO-Fe}_2\text{O}_3\text{-Al}_2\text{O}_3$  system, in particular, in the high-Fe-oxide region would be necessary to improve the illustration of the phase equilibration related to the iron ore sintering process.

#### Acknowledgements

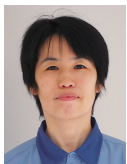
The X-ray absorption measurement was conducted under the collaborative research of the High Energy Accelerator Research Organization (KEK) and Nippon Steel & Sumitomo Metal Corporation (Proposal No. 2015C206). We would like to express our sincere appreciation for Dr. Yoshinori Kitajima, KEK and Mr. Kengo Noami,

Nippon Steel Technology Co., Ltd. for their technical support on the XANES measurement. We would also like to express our gratitude to Prof. Kazumasa Sugiyama from Tohoku University for the fruitful discussion on the crystallographic characteristics of the SFCA phase.

#### References

- 1) Mukherjee, T. et al.: Ironmaking Steelmaking. 12 (4), 151 (1985)
- 2) Inazumi, T.: Iron Ore Sinter: Review of Steps Taken to Overcome the Challenges Posed Japan's Lack of Iron Ore Resources, Tokyo, The Iron and Steel Institute of Japan, 2000
- 3) Van Ende, M.-A. et al.: Metall. Mater. Trans. B. 48 (1), 28 (2017)
- 4) Van Ende, M.-A. et al.: Metall. Mater. Trans. B. 42 (3), 477 (2011)
- 5) Kimura, M. et al.: ISIJ Int. 53 (12), 2047 (2013)
- 6) Kimura, M. et al.: Journal of Physics: Conference Series. 430 (1), 012074 (2013)
- 7) Gröbner, J. et al.: Landolt-Börnstein - Group IV Physical Chemistry. Heidelberg, Springer-Verlag GmbH, 2008

- 8) Kimura, H. et al.: ISIJ Int. 45 (4), 506 (2005)
- 9) Dayal, R.R. et al.: Sci. Ceram. 3, 191 (1967)
- 10) Inoue, K. et al.: Tetsu-to-Hagané. 68 (15), 2190 (1982)
- 11) Hamilton, J.D.G. et al.: N. Jb. Miner. Abh. 161 (1), 1 (1989)
- 12) Mumme, W.G. et al.: N. Jb. Miner. Abh. 173 (1), 93 (1998)
- 13) Mumme, W.G.: N. Jb. Miner. Abh. 178 (3), 307 (2003)
- 14) Sugiyama, K. et al.: ISIJ Int. 45 (4), 560 (2005)
- 15) Murao, R. et al.: ISIJ Int. 58 (2), 259 (2018)
- 16) Lister, D.H. et al.: Br. Ceram. Trans. 66 (7), 293 (1967)
- 17) Patrick, T. et al.: Metall. Mater. Trans. B. 33 (1), 79 (2002)
- 18) Bale, C.W. et al.: Calphad. 26 (2), 189 (2002)
- 19) Decterov, S. et al.: J. Phase Equilib. Diffus. 30 (5), 443 (2009)
- 20) Jung, I.-H.: Calphad. 34 (3), 332 (2010)
- 21) Pelton, A.D. et al.: Metall. Mater. Trans. B. 31 (4), 651 (2000)
- 22) Pelton, A.D. et al.: Metall. Mater. Trans. A. 32 (6), 1355 (2001)
- 23) Hillert, M.: J. Alloys Compd. 320 (2), 161 (2001)
- 24) Hillert, M. et al.: Calphad. 33 (1), 227 (2009)
- 25) Wilke, M. et al.: Am. Mineral. 86 (5-6), 714 (2001)
- 26) Sugiyama, K.: CAMP-ISIJ. 16 (1), 64 (2003)
- 27) Bergman, B.: J. Am. Ceram. Soc. 69 (8), 608 (1986)



Reiko MURAO  
Senior Researcher, Dr. Eng.  
Materials Characterization Research Lab.  
Advanced Technology Research Laboratories  
20-1 Shintomi, Futtsu City, Chiba Pref. 293-8511



In-Ho JUNG  
Associate Professor, Ph.D.  
Dept. of Materials Science and Engineering  
College of Engineering  
Seoul National University



Masao KIMURA  
Professor, Dr. Eng.  
Institute of Materials Structure Science,  
High Energy Accelerator Research Organization  
/School of High Energy Accelerator Science,  
The Graduate University for Advanced Studies